Census: accurate, automated, deep, fast, and hierarchical scRNA-seq cell-type annotation

Bassel Ghaddar[1*] and Subhajyoti De[1*]

[1]Center for Systems and Computational Biology, Rutgers Cancer Institute of New Jersey, Rutgers University; 195 Albany St., New Brunswick, New Jersey 08901
*Correspondence: bassel.ghaddar@gmail.com, sd948@cinj.rutgers.edu

Abstract

We developed Census, an automated, hierarchical cell-type identification method for scRNA-seq data that can deeply annotate normal cells in mammalian tissues and identify malignant cells and their likely cell of origin. When benchmarked on 44 atlas-scale normal and cancer, human and mouse tissues, Census significantly outperforms state-of-the-art methods across multiple metrics. Census is a fast and fully automated method, although users can seamlessly train their own models for customized applications.

Main text

Single cell RNA-seq (scRNA-seq) has enabled annotation and transcriptional characterization of cell-types in multicellular species. Cell-type annotation is a critical and often difficult and time-consuming first step in scRNA-seq data analysis. Typical annotation pipelines involve cell clustering followed by comparison of cluster differentially expressed genes with cell-type marker genes databases[1]. While this approach is suitable for major, well-defined cell-types, it can be challenging to annotate cells from noisy datasets or to identify cell-subtypes for which marker genes are overlapping, poorly expressed, or incompletely described[2,3]. This problem is especially pertinent while analyzing scRNA-seq data from perturbation experiments, disease contexts such as cancer, or treatment conditions.

As such, a number of automated cell identification methods have been developed[4–13], and cell types in many organ-types have been annotated[14,15]. However, when applied to complex tissues, in practice, most suffer from a number of limitations[16–18]. These include inaccurate or shallow annotations, limited organ or cell-type scope, long computation time, the requirement of large reference data, or an inability to distinguish between malignant cells and their normal counterparts[16–18]. In addition, batch effects or differences in cell subtypes between reference and test data often lead to incorrect label predictions or resolutions. Without clearly defined hierarchical cell-type relationships, it can be difficult to identify the appropriate label resolution or alternative cell-type annotations.

To overcome these limitations we developed Census, a fast and fully automated hierarchical cell-type identification method that is conceptually motivated by inherently stratified developmental programs of cellular differentiation. Census implements a collection of hierarchically organized gradient-boosted decision tree models[19] that successively classify individual cells according to a predefined cell hierarchy (**Fig. 1a**). Briefly, Census begins by identifying a cell-type hierarchy from reference scRNA-seq data by hierarchically clustering pseudo-bulk cell-type gene expression data using Ward's method, which splits each node into two child nodes. Next, starting with the root node and for each successive node, differentially expressed genes that distinguish cells from the two child nodes are identified and used as features to train a gradient-boosted tree model to classify the node identity of individual cells. Census uses multiple, relevant percentile-ranked feature scores, allows for missing values, and trains on both full and sparsely down-sampled data, resulting in models that are robust to batch effects.

New datasets are annotated using the pretrained models followed by a custom developed label-stabilizing algorithm (**Fig. 1b**). Census first uses uniform manifold projection and approximation (UMAP) and a shared nearest-neighbor graph[20] to finely cluster data, and it begins by annotating cells with the root classifier. Next, the average label per cluster is propagated and prediction contours in UMAP space are computed. Census resolves disputes within overlapping contour regions and repeatedly redraws contours until the prediction contours stabilize. Given each cell's new identity, the next appropriate node classifier is applied, and this process is repeated until terminal classifications are reached. This is particularly advantageous for organ-scale data with many cell subtypes, both in terms of computation time and classification performance. Census thus leverages multiple design features to achieve high speed and accuracy.

We trained Census to classify 175 cell-types from 24 organs using data from the Tabula Sapiens[14]. Construction of the cell-type hierarchy revealed biologically meaningful groups, with the largest split being immune vs. non-immune cells and with cells further segregating into lymphoid, myeloid, endothelial, stromal, and epithelial groups (**Fig. S1a**). To identify cancer cells, we trained models on scRNA-seq data from 19 cancer types from the Cancer Cell Line Encyclopedia[21] to distinguish malignant cells from organ-specific normal epithelium. The total collection of models had 351 nodes, and all node models had high training classification accuracy (median AUC=0.99, **Fig. S1b**).

We first benchmarked Census against four other state-of-the-art automated annotation methods (scType[4], scATOMIC[5], scibet[6], scCATCH[7]) using a pancreatic cancer dataset[22] that included 57,530 normal and malignant epithelial, stromal, and immune cells. Annotation performance was evaluated by five metrics: F1 score, balanced accuracy, total accuracy, run time, and "label similarity" scores that we computed using our predefined cell hierarchy to quantify closeness of the predicted label to the study's original annotation (see Methods). Census was the top performing method with regards to prediction quality, where it had a higher mean F1 score and balanced accuracy than the second-place method and significantly higher scores than the others (Wilcoxon, $p<0.05$), and it had significantly higher label similarity and accuracy than all methods (Wilcoxon, $p<2e-16$, **Fig. 1c**). While Census was not the fastest method, it ran in 4.5 minutes (range: 1 second-56 minutes, **Fig. 1c**). Census correctly identified 9/10 major cell-types, distinguished between normal and malignant epithelial cells, and identified deeper immune subtypes than originally annotated (**Fig. 1d**).

In terms of accuracy, speed, and precision, Census and scType were the top two methods (**Fig. 1d, Fig. S1c**). We thus proceeded to assess their annotation performance on 44 other challenging normal and cancer datasets from human tissues and from the Tabula Muris[15]; these data included 1,769,071 total cells from 105 harmonized cell labels. In aggregate, Census had significantly higher F1 scores, balanced accuracies, label similarities, and overall accuracies than scType (all Wilcoxon p<2e-16, **Fig. 2a**), although scType had shorter run times (Wilcoxon p<2e-16, **Fig. 2a**) – though Census was still very fast with an average annotation speed of 13,000 cells/minute. Looking at prediction performance in individual studies, Census had higher mean values than scType in 83/100 commonly evaluable metrics (**Fig. 2b**). These data place Census as a top automated annotation method (**Table S1**).

Inspection of specific results highlights the power of Census in diverse settings. In two datasets each of human breast[23,24], colon[25,26], kidney[27,28], liver[29,30], lung[31,32], and pancreas[22,33] cancers, Census identified malignant cells and distinguished them from concurrent normal epithelium (**Fig. 2c-d, Fig. S2a**). It also identified the likely cell of origin for cancer cells. For example, in liver cancer, Census correctly distinguished between known hepatocellular vs. cholangiocarcinoma cells (**Fig. 2d**), in pancreatic cancer it identified most malignant cells as ductal cells and a few tumors as having an acinar cell origin, and in colon cancers the cells of origin were from the enterocyte lineage (**Fig. S2a**). On deeply annotated normal tissue atlases, Census distinguished between several cell subtypes. For example, it identified aerocytes and capillary, vein, artery, and lymphatic endothelial cells, distinguished between alveolar, adventitial, and myo-fibroblasts, and identified several T-cell and myeloid cell subsets in lung[34], colon[35], and heart[36] tissues (**Fig. S2b**). Census also had excellent performance on mouse tissues when tested on droplet and plate-based sequencing samples from the Tabula Muris[15] (**Fig. S2c**), with a mean balanced accuracy of 0.8, label similarity of 0.89, and run time of 13 seconds across all tissues. Overall, Census correctly identified 81/105 tested cell subtypes (compared to 35/89 by scType), and Census's prediction accuracy per cell-type correlated with the corresponding number of cells used for model training (Spearman ρ=0.26, p=0.01).

In summary, Census enables easy and fast, fully-automated cell-type identification from scRNA-seq data using a hierarchical cell-type reference. It significantly outperforms other state-of-the-art methods when extensively tested on human and mouse, cancer and normal tissues. Utilization of a cell-type hierarchy provides a natural interpretation of annotation results and aids in Census's superior performance. It also allows cell type identification at different resolutions, which can be advantageous when comparing results from different datasets, across species, and in the context of complex diseases such as cancer. While the core Census model is trained on the Tabula Sapiens[14], with one line of code users can seamlessly train their own models with other references for customized applications. Census is available on our Github: https://github.com/sjdlabgroup/Census.

Methods

Census algorithm

Constructing the cell-type hierarchy: Census begins by constructing a cell-type hierarchy from reference scRNA-seq data. Given all gene expression and cell-type labels, pseudo-bulk cell-type profiles are created by summing gene counts across all barcodes per cell-type, creating a gene by cell-type table. The resulting profiles are TP10K normalized and then hierarchically clustered using Ward's method, which clusters each node into two leaves. Each node of the hierarchical tree is numbered, and the terminal leaves represent the final cell-types.

Training a Census model: A collection of gradient-boosted tree-based classification models[19] organized by the cell-type hierarchy are next trained to predict cell-type label from scRNA-seq gene expression values. Each node of the cell-type hierarchy has an associated classification model; there are as many models as there are nodes in the cell-type hierarchy. Starting with the root node of the cell-type hierarchy, the cells of all downstream cell-types whose lineage contains the given node are gathered. All nodes bifurcate into two child nodes; the task of the node model of the given node is to classify cells into the appropriate child node of the given node. Cells from the training data are thus given the new identity of their respective child node of the given node through which their lineage runs. This results in two identity classes, and marker genes that distinguish these two classes are identified using Wilcoxon Rank Sum testing, as implemented in Seurat[20]. By default, all statistically significant marker genes are used, although users may impose custom filters or provide alternate marker gene data. The node model uses marker gene counts data to predict the associated cell-label.

Census modifies the training data in three ways before model training. First, zero-values are replaced with NA (not available) to be treated as missing values by the classification algorithm. This is done to account for variable dropout levels across scRNA-seq datasets and across individual cells in a given dataset, wherein zero-values may represent lack of detectable gene expression, low gene expression confounded by measurement noise, or uncaptured gene expression. This also accounts for potentially missing genes between the training data and test datasets, and it takes advantage of the underlying sparsity-aware split finding algorithm developed explicitly by xgboost[19] to optimize handling of missing values in classification problems. Second, gene values for each cell, excluding missing values, are percentile ranked. Third, Census sparsely down-samples this data to create additional training data with more missing values; the default is to supplement the full training data with a 90% sparsified dataset, i.e. a dataset with 90% of values replaced with missing values. The full and sparse training data are combined, and a classification model is trained to predict the cell-label given the gene expression data. This process is repeated for each node of the cell-type hierarchy, with the final models predicting terminal cell-type labels. The above design choices make Census robust to missing values and batch effects.

Annotating cell-types in new datasets: Census uses the resulting models in conjunction with a custom label-stabilizing algorithm to predict new datasets. First, the test dataset is processed using standard scRNA-seq pipelines to project it in two dimensions using uniform manifold projection and approximation (UMAP, i.e. by TP10K normalization, scaling, finding variable genes, computing principle components, and then running the UMAP algorithm using the top principle components), as implemented in Seurat[20]. This data is finely clustered using the first two

UMAP dimensions using a shared nearest-neighbor (SNN) algorithm, as implemented in Seurat[20]. These clusters represent groups of highly similar cells in the test dataset and are used to mitigate prediction error in individual cells. It is crucial at this step that high resolution clustering is done to take advantage of UMAP's preservation of local structure and to avoid co-clustering distant cells.

Next, starting with the first model corresponding to the root node of the cell-type hierarchy, new cell identities are predicted for each individual cell in the test dataset. Census then implements a custom label-stabilizing algorithm that counteracts potential dataset noise and prediction error. First, the average label is propagated within each UMAP SNN cluster. Next, prediction contours are computed on the UMAP plot using the MASS[37] R package. In areas where prediction contours do not overlap, all cells within the contour are given the identity of the contour. In areas where the prediction contours overlap, cells within the overlapping region are given the identity of the most common label in that region. After resolving contour disputes, the most common label is again propagated across each UMAP SNN cluster, and new prediction contours are computed. This process is repeated until either there are no more overlapping prediction contours or until there are no further changes to any cell labels. Each cell now has a new identity, and the next appropriate node model is used to predict subsequent labels; this process is repeated until terminal cell-type classifications are reached. A record of predicted classes and probabilities for each cell in each round of classification is retained.

Census models

The core census model was trained on the Tabula Sapiens[14] to classify 175 cell-types from 24 organs. The cell-type hierarchy contained 345 nodes, with the first node bifurcating into immune vs non-immune cells, and then further branches dividing into B-lymphoid, T-lymphoid, myeloid, endothelial, stromal, and epithelial compartments. The Tabula Sapiens was chosen as the reference for the core model due to its comprehensive human body profiling and consistent cell class ontology labeling, and through extensive benchmarking experiments the core model was found to generalize well across a range of datasets. To predict cancer cells, we trained models on scRNA-seq data from 19 cancer types from the Cancer Cell Line Encyclopedia[21] to distinguish malignant cells from organ-specific normal epithelium. For example, to identify cancer cells in the pancreas, the classification model was trained to distinguish between the cancer cell line data and pancreas epithelium from the Tabula Sapiens, i.e. ductal, acinar, and endocrine cells. When predicting new datasets, the Census model begins by finding terminal classifications for all cell-types using the Tabula Sapiens trained model and cell-type hierarchy. If cancer cells are expected in the sample, then the organ-specific cancer model is applied only to the cells classified as epithelial cells by the Tabula Sapiens model to identify cancer cells. The same contour and cluster-based label stabilizing algorithm is applied. The final output will contain cell-type predictions, and for the predicted cancer cells, and it will also retain the origin normal cell-type prediction as the predicted cell of origin. Cancer cell type models are available for the following organs: breast, colon, kidney, liver, lung, and pancreas. While the Tabula Sapiens and cancer models enable rapid and automated cell-type identification for a variety of datasets, users can also easily train new models with other references (which may include cancer cells as part of the reference) for custom applications.

Benchmarking analyses

Initial benchmarking compared Census to four other state-of-the-art automated annotation methods: scType[4], scATOMIC[5], scibet[6], and scCATCH[7]. For scType, the primary tissue type as well as 'immune system' were chosen for as the tissue type. For scibet, the "30_major_human_cell_types" model was used. Other methods were run with default parameters. All methods were evaluated using on a pancreatic cancer dataset[22]. Census and scType were further evaluated on two datasets each of colon[25,26], kidney[27,28], liver[29,30], lung[31,32], and pancreas[22,33] cancers, normal lung[34], colon[35], and heart[36] datasets, and tissues from the Tabula Muris[15] where applicable. Census was additionally evaluated on two datasets of human breast cancer[23,24]. In total, Census was evaluated on 44 tissue samples from 23 unique tissue types that contained 1,769,071 total cells from 105 harmonized cell labels. To assess performance, F1 scores and balanced accuracies were calculated using the caret R package (https://topepo.github.io/caret/index.html). Label similarity scores to assess closeness of a predicted label to the original author annotated label were calculated as follows. First, cell-type labels from the original studies and the predicted labels from scType[4], scATOMIC[5], scibet[6], and scCATCH[7] were harmonized to the cell ontology annotations used in the Tabula Sapiens[14] using the closest matching label. Then using the cell-type hierarchy created from the Tabula Sapiens, the label similarity score was calculated for each cell-type prediction as the percent of shared nodes of the shorter of the lineages of either the author annotated label or the predicted cell-label. Each individual cell thus had a label-similarity score, and each cell-type from each tissue sample had an F1 score and balanced accuracy. Wilcoxon Rank Sum tests were used to compare metrics for the different cell-type annotation methods.

Statistical analyses

All statistical analyses were performed using R version 3.6.1 (https://www.r-project.org/). The ggpubr package (https://github.com/kassambara/ggpubr) was used to compare group means with nonparametric tests. P-values reported as <2e-16 result from reaching the calculation limit for native R statistical test functions and indicate values below this number, not a range of values. Data processing relied heavily on the Tidyverse v1.3.2 R packages (https://www.tidyverse.org/).

References

1. Clarke, Z. A. *et al.* Tutorial: guidelines for annotating single-cell transcriptomic maps using automated and manual methods. *Nat. Protoc.* **16**, 2749–2764 (2021).

2. Lähnemann, D. *et al.* Eleven grand challenges in single-cell data science. *Genome Biol.* **21**, 31 (2020).

3. Shekhar, K. & Menon, V. Identification of Cell Types from Single-Cell Transcriptomic Data BT - Computational Methods for Single-Cell Data Analysis. in (ed. Yuan, G.-C.) 45–77 (Springer New York, 2019). doi:10.1007/978-1-4939-9057-3_4

4. Ianevski, A., Giri, A. K. & Aittokallio, T. Fully-automated and ultra-fast cell-type identification using specific marker combinations from single-cell transcriptomic data. *Nat. Commun.* **13**, 1246 (2022).

5. Nofech-Mozes, I., Soave, D., Awadalla, P. & Abelson, S. Pan-cancer classification of single cells in the tumour microenvironment. *bioRxiv* 2022.06.14.496107 (2022). doi:10.1101/2022.06.14.496107

6. Li, C. *et al.* SciBet as a portable and fast single cell type identifier. *Nat. Commun.* **11**, 1818 (2020).

7. Shao, X. *et al.* scCATCH: Automatic Annotation on Cell Types of Clusters from Single-Cell RNA Sequencing Data. *iScience* **23**, 100882 (2020).

8. de Kanter, J. K., Lijnzaad, P., Candelli, T., Margaritis, T. & Holstege, F. C. P. CHETAH: a selective, hierarchical cell type identification method for single-cell RNA sequencing. *Nucleic Acids Res.* **47**, e95–e95 (2019).

9. Aran, D. *et al.* Reference-based analysis of lung single-cell sequencing reveals a transitional profibrotic macrophage. *Nat. Immunol.* **20**, 163–172 (2019).

10. Guo, H. & Li, J. scSorter: assigning cells to known cell types according to marker genes. *Genome Biol.* **22**, 69 (2021).

11. Zhang, Y., Zhang, F., Wang, Z., Wu, S. & Tian, W. scMAGIC: accurately annotating single cells using two rounds of reference-based classification. *Nucleic Acids Res.* **50**, e43–e43 (2022).

12. Cortal, A., Martignetti, L., Six, E. & Rausell, A. Gene signature extraction and cell identity recognition at the single-cell level with Cell-ID. *Nat. Biotechnol.* **39**, 1095–1102 (2021).

13. Zhang, A. W. *et al.* Probabilistic cell-type assignment of single-cell RNA-seq for tumor microenvironment profiling. *Nat. Methods* **16**, 1007–1015 (2019).

14. Jones, R. C. *et al.* The Tabula Sapiens: A multiple-organ, single-cell transcriptomic atlas of humans. *Science (80-.).* **376**, (2022).

15. Schaum, N. *et al.* Single-cell transcriptomics of 20 mouse organs creates a Tabula Muris. *Nature* **562**, 367–372 (2018).

16. Abdelaal, T. *et al.* A comparison of automatic cell identification methods for single-cell

RNA sequencing data. *Genome Biol.* **20**, 1–19 (2019).

17. Xie, B., Jiang, Q., Mora, A. & Li, X. Automatic cell type identification methods for single-cell RNA sequencing. *Comput. Struct. Biotechnol. J.* **19**, 5874–5887 (2021).

18. Pasquini, G., Rojo Arias, J. E., Schäfer, P. & Busskamp, V. Automated methods for cell type annotation on scRNA-seq data. *Comput. Struct. Biotechnol. J.* **19**, 961–969 (2021).

19. Chen, T. & Guestrin, C. XGBoost: A Scalable Tree Boosting System. *arXiv* (2016).

20. Stuart, T. *et al.* Comprehensive Integration of Single-Cell Data. *Cell* **177**, 1888-1902.e21 (2019).

21. Kinker, G. S. *et al.* Pan-cancer single-cell RNA-seq identifies recurring programs of cellular heterogeneity. *Nat. Genet.* **52**, 1208–1218 (2020).

22. Peng, J. *et al.* Single-cell RNA-seq highlights intra-tumoral heterogeneity and malignant progression in pancreatic ductal adenocarcinoma. *Nat. Cell Res.* (2019). doi:10.1038/s41422-019-0195-y

23. Wu, S. Z. *et al.* Stromal cell diversity associated with immune evasion in human triple-negative breast cancer. *EMBO J.* **39**, e104063 (2020).

24. Wu, S. Z. *et al.* A single-cell and spatially resolved atlas of human breast cancers. *Nat. Genet.* **53**, 1334–1347 (2021).

25. Pelka, K. *et al.* Spatially organized multicellular immune hubs in human colorectal cancer. *Cell* **184**, 4734-4752.e20 (2021).

26. Lee, H.-O. *et al.* Lineage-dependent gene expression programs influence the immune landscape of colorectal cancer. *Nat. Genet.* **52**, 594–603 (2020).

27. Krishna, C. *et al.* Single-cell sequencing links multiregional immune landscapes and tissue-resident T cells in ccRCC to tumor topology and therapy efficacy. *Cancer Cell* **39**, 662-677.e6 (2021).

28. Bi, K. *et al.* Tumor and immune reprogramming during immunotherapy in advanced renal cell carcinoma. *Cancer Cell* **39**, 649-661.e5 (2021).

29. Ma, L. *et al.* Single-cell atlas of tumor cell evolution in response to therapy in hepatocellular carcinoma and intrahepatic cholangiocarcinoma. *J. Hepatol.* **75**, 1397–1408 (2021).

30. Massalha, H. *et al.* A single cell atlas of the human liver tumor microenvironment. *Mol. Syst. Biol.* **16**, e9682 (2020).

31. Wu, F. *et al.* Single-cell profiling of tumor heterogeneity and the microenvironment in

advanced non-small cell lung cancer. *Nat. Commun.* **12**, 2540 (2021).

32. Kim, N. *et al.* Single-cell RNA sequencing demonstrates the molecular and cellular reprogramming of metastatic lung adenocarcinoma. *Nat. Commun.* **11**, 2285 (2020).
33. Hwang, W. L. *et al.* Single-nucleus and spatial transcriptome profiling of pancreatic cancer identifies multicellular dynamics associated with neoadjuvant treatment. *Nat. Genet.* **54**, 1178–1191 (2022).
34. Travaglini, K. J. *et al.* A molecular cell atlas of the human lung from single-cell RNA sequencing. *Nature* **587**, 619–625 (2020).
35. Smillie, C. S. *et al.* Intra- and Inter-cellular Rewiring of the Human Colon during Ulcerative Colitis. *Cell* **178**, 714-730.e22 (2019).
36. Litviňuková, M. *et al.* Cells of the adult human heart. *Nature* **588**, 466–472 (2020).
37. Veneables, W. & Ripley, B. *Modern Applied Statistics with S*. (Springer US, 2002).

Supplementary Materials

Table S1. Evaluation metrics for benchmarking experiments

Acknowledgments

We acknowledge the Office of Advanced Research Computing (OARC) at Rutgers, The State University of New Jersey for providing access to the Amarel cluster URL: https://it.rutgers.edu/oarc.

Funding

National Institutes of Health grant R21CA248122 (SD)
National Institutes of Health, National Center for Advancing Translational Sciences, Rutgers Clinical and Translational Science Award TL1TR003019 (BG)

Author contributions

BG conceived the study. BG designed and performed all data analyses. BG and SD interpreted the data and wrote and revised the manuscript.

Competing interests

The authors declare no competing interests.

Data and materials availability:

Census is available on our Github: https://github.com/sjdlabgroup/Census. Other data and code are available from the authors upon reasonable request.

Figure Legends

Figure 1. Overview of Census and initial benchmarking. a, Schematic diagram of training a Census model. The default Census model is trained on the Tabula Sapiens and Cancer Cell Line Encyclopedia. **b,** Schematic diagram of the Census prediction method and label-stabilizing algorithm. **c,** Benchmarking Census against four other automated cell-type annotation methods using a pancreatic cancer dataset. Boxplots show median (line), 25th and 75th percentiles (box) and 1.5xIQR (whiskers). Points represent outliers; Wilcoxon tests, **** p<1e-4; *** p<1e-3; ** p<1e-2, * p<0.05; ns, not significant. **d,** Uniform manifold approximation and projection (UMAP) plots of 57,530 cells from a pancreatic cancer study colored by cell-type with overlaid labels. Left, original study annotations, middle, Census annotations, right, scType annotations. HSC/MPP, hematopoietic/multipotent progenitor.

Figure 2. Extended benchmarking of Census on normal and cancer, human and mouse tissues. a, Performance metrics comparing Census and scType on 25 tissues. Boxplots show median (line), 25th and 75th percentiles (box) and 1.5xIQR (whiskers). Points represent outliers; Wilcoxon tests, **** p<1e-4. **b,** Heatmap showing the top performing method across four evaluation metrics for 25 commonly evaluable tissues. Green color, Census had a higher mean value, yellow color, scType had a higher mean value. tm, Tabula Muris **c,** Example uniform manifold approximation and projection (UMAP) plots of 167,283 cells from a clear cell renal cell carcinoma (ccRCC) study colored by cell-type with overlaid labels. Left, original study annotations, middle, Census annotations, right, Census cancer cell of origin prediction. TAM, tumor associated macrophage; DC, dendritic cell, Treg; regulatory T-cell. **d,** Example UMAP plots of 57,000 cells from a liver cancer (LC) study colored by cell-type with overlaid labels. Left, original study annotations, middle, Census annotations, right, Census cancer cell of origin prediction. TAM, tumor associated macrophage; TEC, tumor endothelial cell, CAF, cancer associated fibroblast.

Figure S1. Tabula Sapiens cell-type hierarchy and benchmarking data. a, Dendrogram plotting the cell-type hierarchy derived from the Tabula Sapiens. Cells are colored by major compartment; blue, lymphoid; purple, myeloid; red, stromal; orange, epithelial. **b,** Histogram of receiver operator areas under the curves (AUC) for all nodes during Tabula Sapiens model training. **c,** Uniform manifold approximation and projection (UMAP) plots of 57,530 cells from a pancreatic cancer study colored by predicted cell-type with overlaid labels.

Figure S2. Evaluating Census on human and mouse datasets. a, Uniform manifold approximation and projection (UMAP) plots of 12 cancer datasets colored by cell-type annotation with overlaid labels. Left, original author annotations; middle, Census annotation; right, Census predicted cancer cell of origin. PDAC, pancreatic ductal adenocarcinoma; RCC, renal cell carcinoma; ccRCC, clear cell renal cell carcinoma; LUAD, lung adenocarcinoma; BC, breast

cancer; NSCLC, non-small cell lung cancer; CRC, colorectal cancer; LC, liver cancer. **b,** UMAP plots of Census annotations on normal human lung, colon, and heart tissues colored by cell-type and with overlaid labels. Left, original author annotations; right, Census annotation. **c,** Evaluating Census prediction performance on tissues from the Tabula Muris. Boxplots show median (line), 25th and 75th percentiles (box) and 1.5xIQR (whiskers). Points represent outliers.

Figure 1

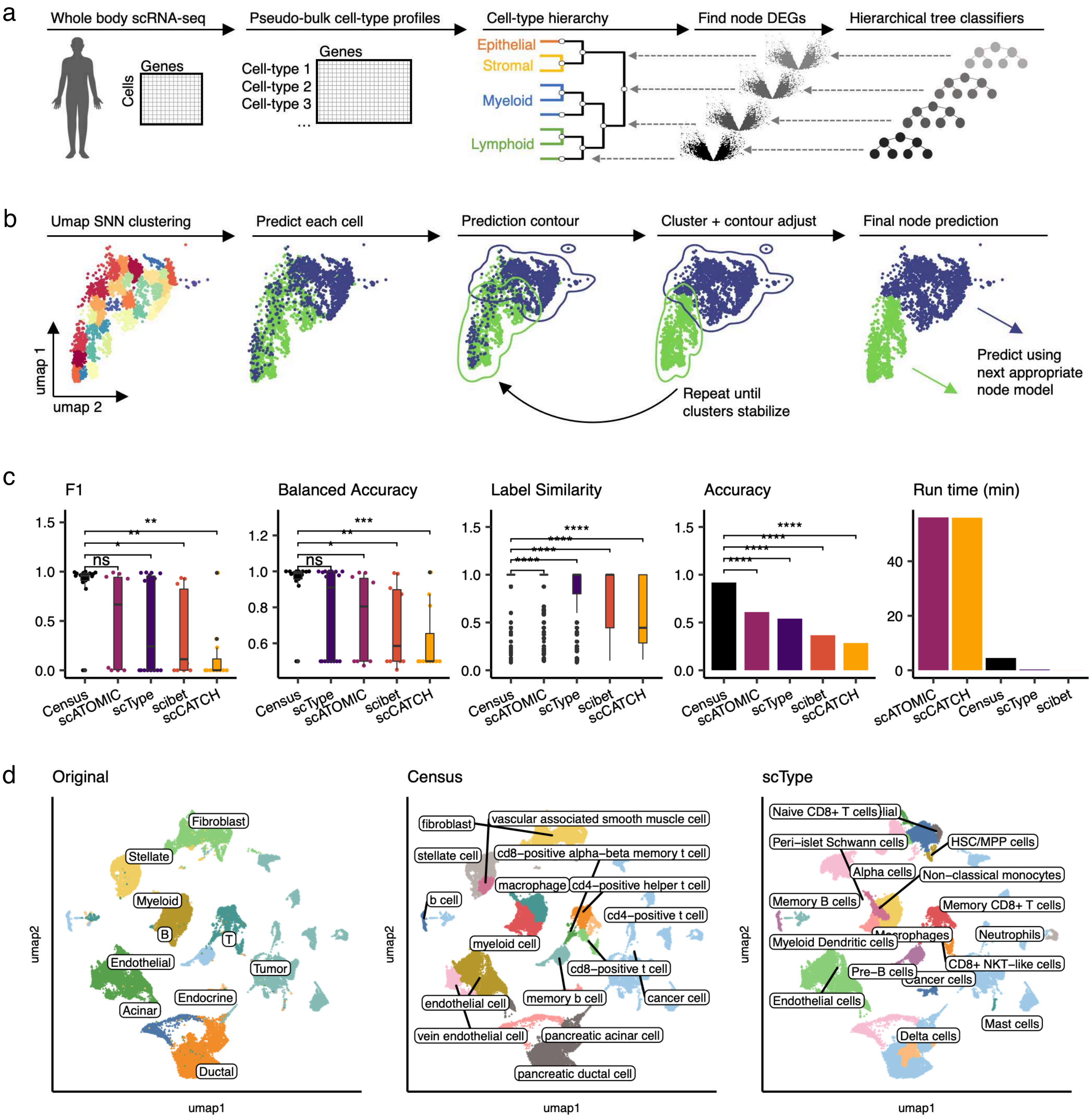
a
Whole body scRNA-seq
Cells
Genes
Pseudo-bulk cell-type profiles
Genes
Cell-type 1
Cell-type 2
Cell-type 3
...
Cell-type hierarchy
Epithelial
Stromal
Myeloid
Lymphoid
Find node DEGs
Hierarchical tree classifiers
b
Umap SNN clustering
umap 1
umap 2
Predict each cell
Prediction contour
Cluster + contour adjust
Repeat until clusters stabilize
Final node prediction
Predict using next appropriate node model
c
F1
1.5
1.0
0.5
0.0
ns
*
**
**
Census
scATOMIC
scType
scibet
scCATCH
Balanced Accuracy
1.2
1.0
0.8
0.6
ns
*
**
***
Census
scType
scATOMIC
scibet
scCATCH
Label Similarity
1.5
1.0
0.5
0.0
****
****
****
****
Census
scATOMIC
scType
scibet
scCATCH
Accuracy
1.5
1.0
0.5
0.0
****
****
****
****
Census
scATOMIC
scType
scibet
scCATCH
Run time (min)
40
20
0
scATOMIC
scCATCH
Census
scType
scibet
d
Original
Fibroblast
Stellate
Myeloid
B
T
Endothelial
Tumor
Endocrine
Acinar
Ductal
umap2
umap1
Census
fibroblast
vascular associated smooth muscle cell
stellate cell
cd8−positive alpha−beta memory t cell
b cell
macrophage
cd4−positive helper t cell
cd4−positive t cell
myeloid cell
cd8−positive t cell
endothelial cell
memory b cell
cancer cell
vein endothelial cell
pancreatic acinar cell
pancreatic ductal cell
umap2
umap1
scType
Naive CD8+ T cells
lial
Peri−islet Schwann cells
HSC/MPP cells
Alpha cells
Non−classical monocytes
Memory B cells
Memory CD8+ T cells
Macrophages
Neutrophils
Myeloid Dendritic cells
CD8+ NKT−like cells
Pre−B cells
Cancer cells
Endothelial cells
Mast cells
Delta cells
umap2
umap1

Figure 2

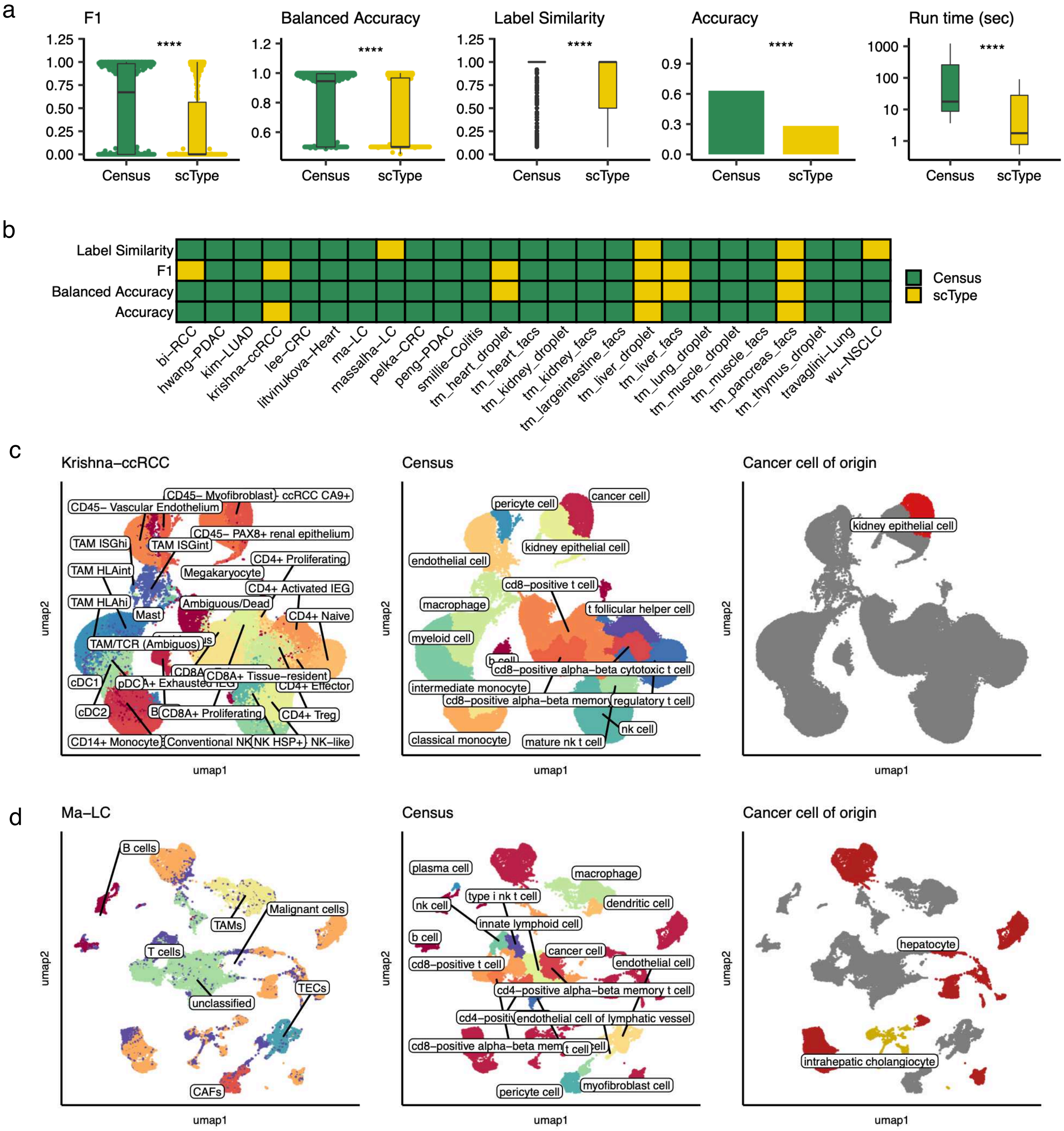
a
F1
1.25
1.00
0.75
0.50
0.25
0.00
****
Census
scType
Balanced Accuracy
1.2
1.0
0.8
0.6
****
Census
scType
Label Similarity
1.25
1.00
0.75
0.50
0.25
0.00
****
Census
scType
Accuracy
0.9
0.6
0.3
0.0
****
Census
scType
Run time (sec)
1000
100
10
1
****
Census
scType
b
Label Similarity
F1
Balanced Accuracy
Accuracy
🟩 Census
🟨 scType
bi–RCC
hwang–PDAC
kim–LUAD
krishna–ccRCC
lee–CRC
litvinukova–Heart
ma–LC
massalha–LC
pelka–CRC
peng–PDAC
smillie–Colitis
tm_heart_droplet
tm_heart_facs
tm_kidney_droplet
tm_kidney_facs
tm_largeintestine_facs
tm_liver_droplet
tm_liver_facs
tm_lung_droplet
tm_muscle_droplet
tm_muscle_facs
tm_pancreas_facs
tm_thymus_droplet
travaglini–Lung
wu–NSCLC
c
Krishna–ccRCC
CD45– Myofibroblast
ccRCC CA9+
CD45– Vascular Endothelium
CD45– PAX8+ renal epithelium
TAM ISGhi
TAM ISGint
CD4+ Proliferating
TAM HLAint
Megakaryocyte
CD4+ Activated IEG
TAM HLAhi
Ambiguous/Dead
Mast
CD4+ Naive
TAM/TCR (Ambiguos)
CD8A
CD8A+ Tissue–resident
cDC1
pDC
A+ Exhausted IEG
CD4+ Effector
cDC2
B
CD8A+ Proliferating
CD4+ Treg
CD14+ Monocyte
Conventional NK
NK HSP+
NK–like
umap2
umap1
Census
pericyte cell
cancer cell
kidney epithelial cell
endothelial cell
cd8–positive t cell
macrophage
t follicular helper cell
myeloid cell
b cell
cd8–positive alpha–beta cytotoxic t cell
intermediate monocyte
cd8–positive alpha–beta memory
regulatory t cell
nk cell
classical monocyte
mature nk t cell
umap2
umap1
Cancer cell of origin
kidney epithelial cell
umap2
umap1
d
Ma–LC
B cells
Malignant cells
TAMs
T cells
TECs
unclassified
CAFs
umap2
umap1
Census
plasma cell
macrophage
type i nk t cell
nk cell
dendritic cell
innate lymphoid cell
b cell
cancer cell
cd8–positive t cell
endothelial cell
cd4–positive alpha–beta memory t cell
cd4–positi
endothelial cell of lymphatic vessel
cd8–positive alpha–beta mem
t cell
ell
pericyte cell
myofibroblast cell
umap2
umap1
Cancer cell of origin
hepatocyte
intrahepatic cholangiocyte
umap2
umap1

Figure S1

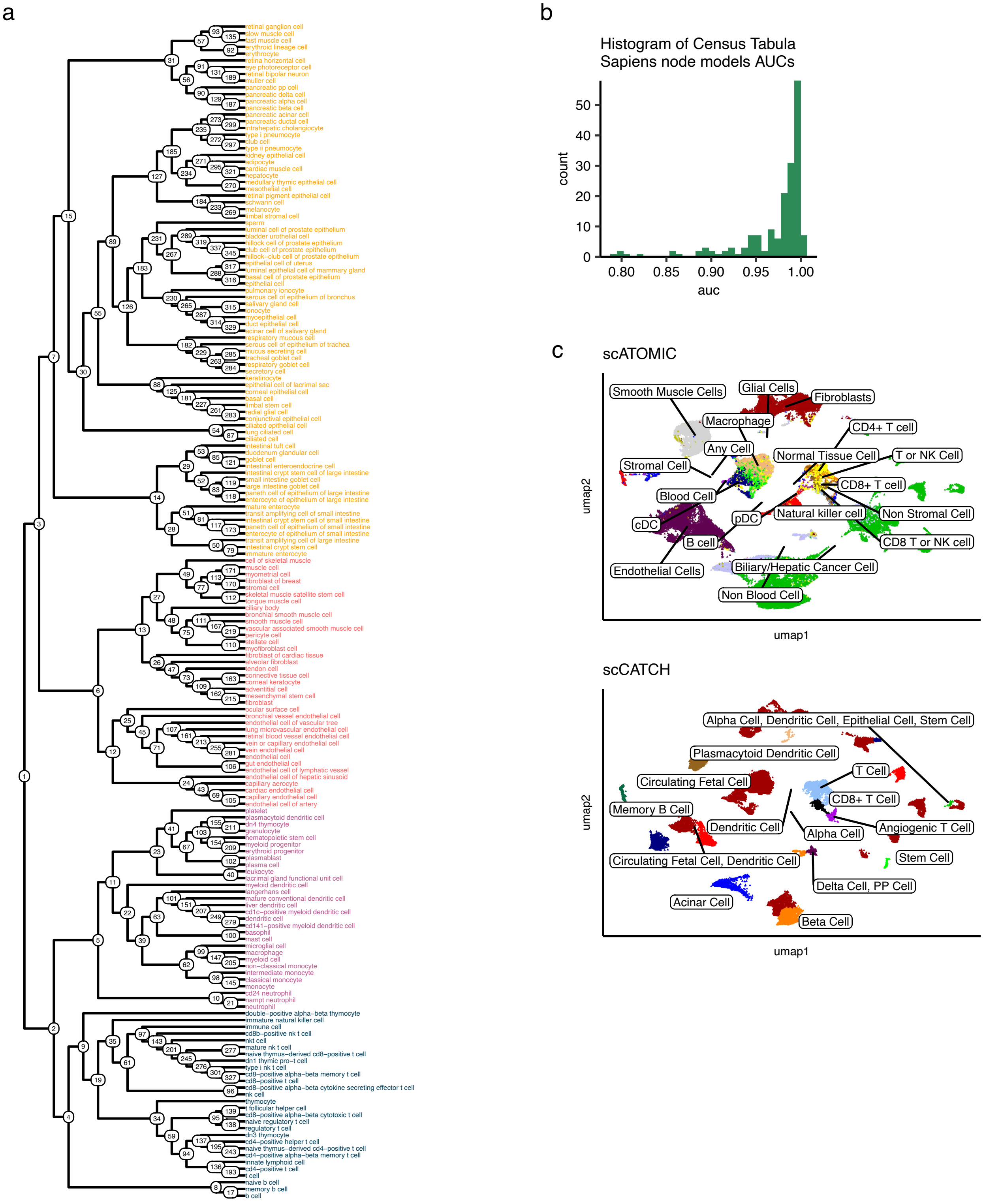
a
retinal ganglion cell
slow muscle cell
fast muscle cell
erythroid lineage cell
erythrocyte
retina horizontal cell
eye photoreceptor cell
retinal bipolar neuron
muller cell
pancreatic pp cell
pancreatic delta cell
pancreatic alpha cell
pancreatic beta cell
pancreatic acinar cell
pancreatic ductal cell
intrahepatic cholangiocyte
type i pneumocyte
club cell
type ii pneumocyte
kidney epithelial cell
adipocyte
cardiac muscle cell
hepatocyte
medullary thymic epithelial cell
mesothelial cell
retinal pigment epithelial cell
schwann cell
melanocyte
limbal stromal cell
sperm
luminal cell of prostate epithelium
bladder urothelial cell
hillock cell of prostate epithelium
club cell of prostate epithelium
hillock–club cell of prostate epithelium
epithelial cell of uterus
luminal epithelial cell of mammary gland
basal cell of prostate epithelium
epithelial cell
pulmonary ionocyte
serous cell of epithelium of bronchus
salivary gland cell
ionocyte
myoepithelial cell
duct epithelial cell
acinar cell of salivary gland
respiratory mucous cell
serous cell of epithelium of trachea
mucus secreting cell
tracheal goblet cell
respiratory goblet cell
secretory cell
keratinocyte
epithelial cell of lacrimal sac
corneal epithelial cell
basal cell
limbal stem cell
radial glial cell
conjunctival epithelial cell
ciliated epithelial cell
lung ciliated cell
ciliated cell
intestinal tuft cell
duodenum glandular cell
goblet cell
intestinal enteroendocrine cell
intestinal crypt stem cell of large intestine
small intestine goblet cell
large intestine goblet cell
paneth cell of epithelium of large intestine
enterocyte of epithelium of large intestine
mature enterocyte
transit amplifying cell of small intestine
intestinal crypt stem cell of small intestine
paneth cell of epithelium of small intestine
enterocyte of epithelium of small intestine
transit amplifying cell of large intestine
intestinal crypt stem cell
immature enterocyte
cell of skeletal muscle
muscle cell
myometrial cell
fibroblast of breast
stromal cell
skeletal muscle satellite stem cell
tongue muscle cell
ciliary body
bronchial smooth muscle cell
smooth muscle cell
vascular associated smooth muscle cell
pericyte cell
stellate cell
myofibroblast cell
fibroblast of cardiac tissue
alveolar fibroblast
tendon cell
connective tissue cell
corneal keratocyte
adventitial cell
mesenchymal stem cell
fibroblast
ocular surface cell
bronchial vessel endothelial cell
endothelial cell of vascular tree
lung microvascular endothelial cell
retinal blood vessel endothelial cell
vein or capillary endothelial cell
vein endothelial cell
endothelial cell
gut endothelial cell
endothelial cell of lymphatic vessel
endothelial cell of hepatic sinusoid
capillary aerocyte
cardiac endothelial cell
capillary endothelial cell
endothelial cell of artery
platelet
plasmacytoid dendritic cell
dn4 thymocyte
granulocyte
hematopoietic stem cell
myeloid progenitor
erythroid progenitor
plasmablast
plasma cell
leukocyte
lacrimal gland functional unit cell
myeloid dendritic cell
langerhans cell
mature conventional dendritic cell
liver dendritic cell
cd1c–positive myeloid dendritic cell
dendritic cell
cd141–positive myeloid dendritic cell
basophil
mast cell
microglial cell
macrophage
myeloid cell
non–classical monocyte
intermediate monocyte
classical monocyte
monocyte
cd24 neutrophil
nampt neutrophil
neutrophil
double–positive alpha–beta thymocyte
immature natural killer cell
immune cell
cd8b–positive nk t cell
nkt cell
mature nk t cell
naive thymus–derived cd8–positive t cell
dn1 thymic pro–t cell
type i nk t cell
cd8–positive alpha–beta memory t cell
cd8–positive t cell
cd8–positive alpha–beta cytokine secreting effector t cell
nk cell
thymocyte
t follicular helper cell
cd8–positive alpha–beta cytotoxic t cell
naive regulatory t cell
regulatory t cell
dn3 thymocyte
cd4–positive helper t cell
naive thymus–derived cd4–positive t cell
cd4–positive alpha–beta memory t cell
innate lymphoid cell
cd4–positive t cell
t cell
naive b cell
memory b cell
b cell
b
Histogram of Census Tabula
Sapiens node models AUCs
count
auc
0
10
20
30
40
50
0.80
0.85
0.90
0.95
1.00
c
scATOMIC
Smooth Muscle Cells
Glial Cells
Fibroblasts
Macrophage
CD4+ T cell
Any Cell
Stromal Cell
Normal Tissue Cell
T or NK Cell
CD8+ T cell
Blood Cell
pDC
Natural killer cell
Non Stromal Cell
cDC
B cell
CD8 T or NK cell
Endothelial Cells
Biliary/Hepatic Cancer Cell
Non Blood Cell
umap2
umap1
scCATCH
Alpha Cell, Dendritic Cell, Epithelial Cell, Stem Cell
Plasmacytoid Dendritic Cell
Circulating Fetal Cell
T Cell
CD8+ T Cell
Memory B Cell
Dendritic Cell
Alpha Cell
Angiogenic T Cell
Circulating Fetal Cell, Dendritic Cell
Stem Cell
Delta Cell, PP Cell
Acinar Cell
Beta Cell
umap2
umap1

Figure S2

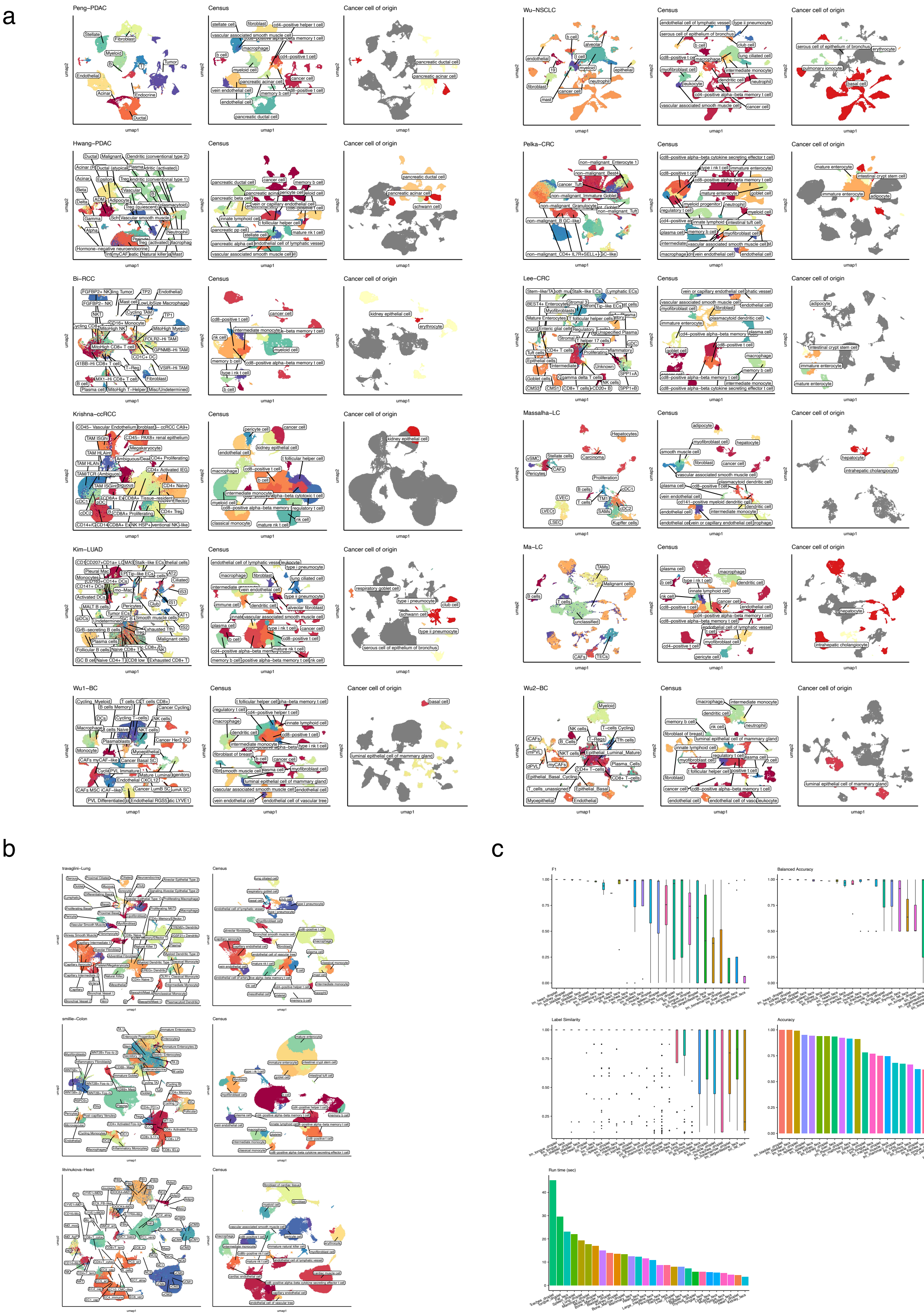
a
Peng–PDAC
Census
Cancer cell of origin
Wu–NSCLC
Hwang–PDAC
Pelka–CRC
Bi–RCC
Lee–CRC
Krishna–ccRCC
Massalha–LC
Kim–LUAD
Ma–LC
Wu1–BC
Wu2–BC
umap1
umap2
b
travaglini–Lung
smillie–Colon
litvinukova–Heart
c
F1
Balanced Accuracy
Label Similarity
Accuracy
Run time (sec)